JMEPEG (1997) 6:223-239

Ion Implantation and Diamond-Like Coatings of Aluminum Alloys

G.W. Malaczynski, A.H. Hamdi, A.A. Elmoursi, and X. Qiu

In an attempt to increase the wear resistance of some key automotive components, General Motors Research and Development Center initiated a study to determine the potential of surface modification as a means of improving the tribological properties of automotive parts, and to investigate the feasibility of mass producing such parts. This paper describes the plasma immersion ion implantation system that was designed for the study of various options for surface treatment, and it discusses bench testing procedures used for evaluating the surface-treated samples. In particular, both tribological and microstructural analyses are discussed for nitrogen implants and diamond-like hydrocarbon coatings of some aluminum alloys.

Keywords

aluminum alloys, diamond-like hydrocarbon, ion implantation, wear resistant coating

1. Introduction

THE USE OF ION BEAMS for metallic surface modification has shown promising results in several applications (Ref 1-4). The high cost of conventional line-of-sight ion implantation, however, is the main obstacle to its extensive use on an industrial scale. The recent development of plasma immersion ion implantation (PIII) at the University of Wisconsin at Madison (Ref 5) has offered the potential to reduce the cost of implantation and has enabled surface modification of three-dimensional structures on an industrial scale. In this IONCLAD process, the name adopted by General Motors, ions which surround the workpiece in the form of a plasma are accelerated into the workpiece under the influence of a high-voltage pulse. Hence, target manipulation is not required. An additional benefit is that the ion incidence is almost always perpendicular to the treated surface, which improves the dose uniformity, even over a complex-shaped surface. This new method allows for simultaneous treatment of multiple items, provided that the spacing of the workpieces is not so small that they compete for access to the plasma. This batch processing technique substantially increases throughput and, thus, substantially could reduce the cost to a commercially viable level.

In 1990 the General Motors Research and Development Center initiated an effort to build a PIII system in order to study the potential for modifying the tribological properties of automotive parts and to investigate the feasibility of producing surface-modified components. Concurrent with this effort to construct an implanter, candidate materials of substantial importance to the automotive industry were investigated. This effort was supported by the Center's Metallurgy Department, which has an extensive background in the measurement of wear and corrosion properties of materials.

This article describes the key components of the PIII system and gives an overview of the project. In addition, some justification for the choice of the components is given, in the hope that a brief discussion of the principal features of the experiment will highlight the problems which are encountered when experimenting with PIII. Since, in general, PIII is a multidisciplinary project requiring knowledge of high-voltage engineering, vacuum technology, plasma physics, material science, and tribology, some diagnostic techniques allowing for the assessment of the quality of surfaces modified with PIII are also given. This leads to the presentation of some preliminary results and finally to a discussion of the scope and applicability of the method.

G.W. Malaczynski, A.H. Hamdi, A.A. Elmoursi, and **X. Qiu**, General Motors Research and Development Center, Electrical and Electronics Engineering Dept., 30500 Mound Rd., Warren, MI 48090-9055, USA.

2. The Experimental System

2.1 *Reaction Chamber*

The main chamber is a 1 m^3 stainless steel cube (see Fig. 1a and 1b) with standard-size ports for a vacuum system consisting of cryogenically cooled (cryo), turbomechanical (turbo), and mechanical (roughing) pumps located below the base of the chamber. The cryo pump is used for initial evacuation of the system to a base pressure on the order of 10^{-8} torr and for "clean" experiments. In most cases, however, a turbo pump provides an adequate environment for implantation or deposition without the inconvenience of periodic shut-down necessary for cryo pump recovery. An access port is provided in the form of a hinged front door for ease of loading. A number of standard conflat ports located on every side of the cube are included to accommodate plasma and implantation process diagnostic tools. There is a provision for attaching a plasma source at each side of the cube, except the bottom, in order to verify the effectiveness of a multi-source system and coexistence of various sources. To avoid excessive charge recombination at the main chamber's wall, a magnetic plasma confinement system was employed in the form of segmented subassemblies (see Fig. 2) carrying MAGNEQUENCH-3 rare-earth permanent magnets whose exceptional energy product (35×10^6 G · Oe, compared to one order of magnitude lower for ferrite magnets) compensate for locating them outside the chamber. Location of the magnets outside the vacuum chamber secures flexibility in experimenting with various arrays of the permanent magnets and prevents additional contamination and outgassing problems in the chamber.

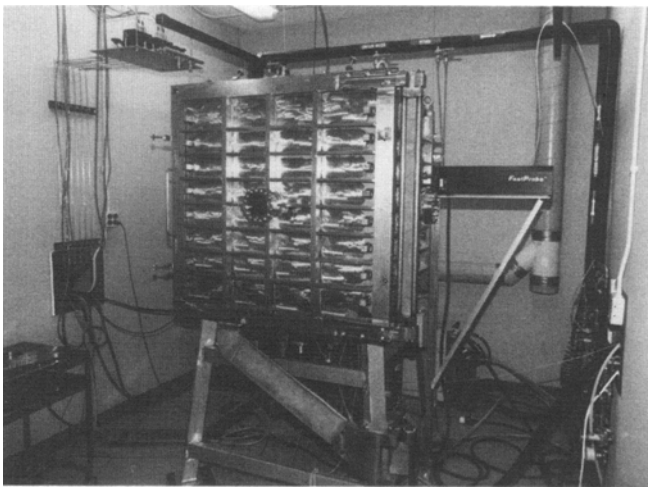

(a)

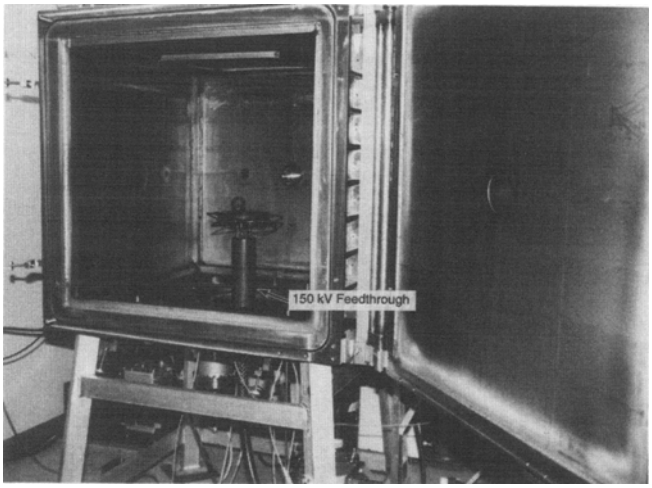

(b)

Fig. 1 (a) The General Motors Research and Development Center IONCLAD system assembly. (b) Interior of the 1 m^3 vacuum chamber showing 150 kV feedthrough

A target table, electrically insulated from the ground so as to withstand the high voltage pulses, is supported by a 150 kV feedthrough which delivers the electric energy to the table. The target temperature, which might rise due to the heating effect of intense ion bombardment, is controlled by coolant circulation from a multi-kilowatt heat exchanger through this custom-designed high-voltage feedthrough.

The plasma diagnostic system consists of a single Langmuir probe. In order to obtain a plasma profile along the distance between the wall and the center of the main chamber, a fast-injection probe system provided by Plasma and Material Science Technologies, Inc. is employed. It provides up to 40 plasma I-V characteristics per probe injection, by sweeping a probe bias voltage in the required polarity range with a frequency of 200 Hz over the probe's stroke distance of 30 cm.

2.2 *High Voltage Pulser*

The high voltage pulse applied to the target must comply with numerous requirements in order to achieve the desired implantation efficiency and flexibility in tailoring the implantation process itself (see, e.g., Ref 5-8).

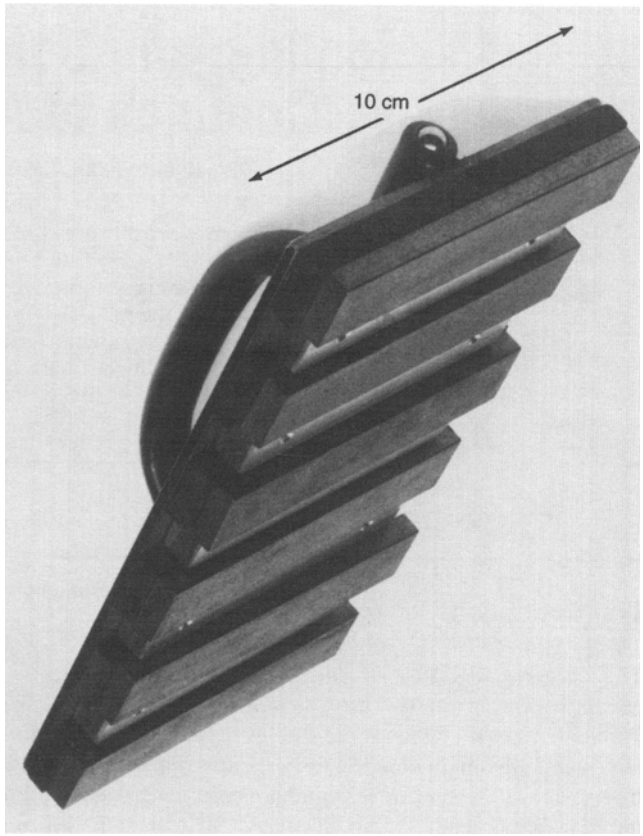

Fig. 2 Magnet subassembly allowing for fast rearrangement of various magnetic field patterns

In general, as square a pulse as possible is desired to simplify any theoretical analysis and to achieve the maximum, most uniform acceleration of the ions over the pulse duration. However, in practice, even a very carefully designed pulse source will, to a certain extent, be corrupted by the plasma dynamic load impedance, which is highly variable and may span several decades over the pulse duration. Evolvement of the plasma impedance in time reflects a rather complex chain of events, because it is the result of the creation of an electrically non-neutral region formed between the plasma and the target the very moment an electric bias is applied to the target. The maximum capacitance of the load is defined by the initial distance between the still-unbiased target and the undisturbed plasma (the Debye length). The moment the pulse is applied to the target, the charge separation process redefines this distance. In the other limit (minimum load capacitance), the capacitance is defined by the position of the expanding plasma sheath at the pulse termination. A rough calculation indicates that early in time the load capacitance may reach several nanofarads, while toward the pulse end it might be on the order of tens of picofarads. The plasma dynamic resistance is much more difficult to assess. It is a function determined by the space-charge limited conduction current, sheath expansion, and secondary electron emission. Therefore, it will vary with gas type, its degree of ionization, and the composition of the target material.

In effect, it is expected that, at the early stage of the applied high voltage pulse, a displacement current surge will shape the slope of the voltage pulse. A properly designed power source must withstand the dynamics of the plasma impedance, since the plasma resistance increase over the pulse duration is on the order of one order of magnitude and is partly compensated by the decrease of the plasma sheath capacitance (see, e.g., Ref 7). Optimal pulse-modulator design criteria for the PIII application, therefore, are believed to be rather demanding and depend on the application, since the target (workpiece or workpieces) and chamber geometries are a portion of the equation. In addition, a production-oriented environment most likely would require a high-production throughput rate, which translates to a high pulse repetition rate together with a large implant area. This implies an ability to efficiently switch high electric power at high voltage and current levels.

Laboratory experiments usually involve systems featuring high flexibility due to constantly changing demands. The relatively early experimental stage and the developmental aspects of the PIII process make the construction of a flexible PIII system a formidable task. A compromise was achieved by specifying a set of desired features which make the experimental system flexible enough for the research portion of the project without losing the chance to investigate and ultimately demonstrate the feasibility of the modulator in a production environment. The above considerations resulted in the following specification for the high voltage pulser adopted for the PIII experiments:

- Negative polarity with variable output pulse amplitude from 500 V to 150 kV
- Pulse repetition rate 10 Hz to 10 kHz
- Pulse width, variable, 10 to 30 μs
- Pulse rise time (10 to 90%), better than 3 μs
- Pulse fall time (10 to 90%), better than 5 μs
- Load resistance, variable, not less than 600 Ω and not more than 30 kΩ
- Load capacitance, variable, 60 to 1000 pF.

The above specification substantially compromises the rise and fall time requirements, but at least at lower plasma densities, it should not impair the implantation properties. At higher plasma densities, however, fall times become more critical and contribute to substantial sputtering caused by low energy ions driven to the target by the pulse tail. The rise time, on the other hand, contributes to the initial displacement current surge, but a reasonable compromise reduces system driver power without any substantial deterioration in the implant quality.

An excellent review of high-voltage pulse technology suitable for PIII applications is given in Ref 6. For large-scale operations the amortized system cost, consisting of factors such as reliability, routine maintenance, and electrical efficiency, must be considered. Therefore, the optimization of pulser performance becomes an independent issue and requires a separate effort. In practice, manufacturing requirements lead to a specification list which demands a combination of low cost, only routine maintenance, and long component life, all securing reasonable investment and exploitation costs. Usually, these requirements are met at the expense of system flexibility, which is almost always the most desirable feature in the development stage. Early-stage experiment requirements regarding the system power, dictated by the load impedance variation, pulse repetition, and voltage range, limited the choice to a thyratron switched pulse forming network (PFN), supported by a step-up pulse transformer. Gaseous switch tube modulators are well understood and can be easily modified if necessity arrives. By no means, however, should a thyratron switch be considered for a mass production application, because the life of its critical components is relatively short, especially under conditions of notorious load impedance mismatch due to the changing plasma conditions over the pulse duration.

In the pulse modulator assembly used for the experiments discussed here, two LS-4101 thyratrons are employed, one operating to switch the PFN and the other to crowbar the pulse. A thyratron acting as an output switch connects the PFN into a pulse transformer having a step-up ratio of 1:10. With the PFN fully charged by a suitable direct current (DC) power unit, the pulse modulator delivers a 150 kV negative polarity to the 30 kΩ load at repetition rates up to 200 Hz. Since the PFN is designed for a fixed pulse width, the variable pulse widths are obtained by crowbarring the PFN-generated pulse at the appropriate time into the pulse by the second thyratron switch connected to ground through a dumping resistor. For experiments with higher plasma density, the pulser architecture was rearranged. A pulse transformer having a step-up ratio of 1:2 was employed, which delivers 30 kV to the 600 Ω load, or the whole PFN was replaced, allowing for delivery of 120 kV pulses (with maximum repetition rate of 80 Hz) to 2 kΩ load with the assistance of a 1:10 step-up transformer. An ultimate limit for the power delivered to the implanted target was an upper limit of the available DC power supply equal to 8 kJ/s.

3. Bench Test for Evaluating Surface-Treated Materials

A bench test was developed that allows the evaluation of friction and resistance to wear of the modified materials. A wide range of variables seemingly important for the measurement of friction can be studied employing a pin-on-disk tribometer. This bench test method can be used not only for evaluating new surface treatments, but also for understanding the tribological mechanisms between any two material surfaces. Knowledge of the tribological behavior of the base material should be used as a reference base to evaluate surface modification effects on the tribological properties of materials. It might be possible to find a quantifiable criterion for ranking the performance of different materials, including some existing materials as well as implanted surfaces. Using both a pin-on-disk and a reciprocating tribometer, we hoped to establish bench test methods to evaluate the tribological properties of materials couples in friction.

3.1 *Pin-on-Disk Tribometer Bench Test Procedure*

The friction and the scuffing-related friction behavior (i.e., material transfer) of aluminum 390 surface-modified derivatives, and cast iron or aluminum 390 alloy, have been systematically studied. The latter two are considered base materials. A

wide range of variables critical for the consistency of measurement of friction, performed with the pin-on-disk tribometer, have been carefully studied and led to tentative guidelines for tribology testing:

- Given enough time, scuffing will always occur under dry (unlubricated) conditions, even if the pair aluminum/cast iron (the best performer) is selected for the test. Therefore, at constant load, the duration of the test, and consequently the time to failure, become important indicators of the material's resistance to wear/scuff.
- Differentiation of the performance of different couples becomes highly unreliable when the tested couple is lubricated.
- Without any lubrication, the aluminum alloy/aluminum alloy (Al/Al) couple always scuffs, almost immediately, regardless of the testing conditions (load, humidity, etc.)
- The critical friction coefficient, above which scuffing is most likely to occur, is in the range of 0.6 to 0.8. Knowledge of this critical range provides a screening tool for material selection. Change in sliding speed, between 10 and 24 cm/s, did not seem to affect the friction measurement in our tests.

The above observations define the standard test conditions which were maintained when testing surface-modified materials. However, in general, precise friction coefficient readings can vary with contact pressure, sliding speed, rotation rate, temperature, humidity, type of tribometer, surface finish of the material couple, etc. (see, e.g., Ref 9-11). Therefore, all other parameters which were not controllable during the experiments contribute to the deviation in the value of measured coefficient of friction. Despite this shortcoming, the test results led to establishing a low-friction (safe operation) zone and a failure zone. These areas were separated by an area of uncertainty,

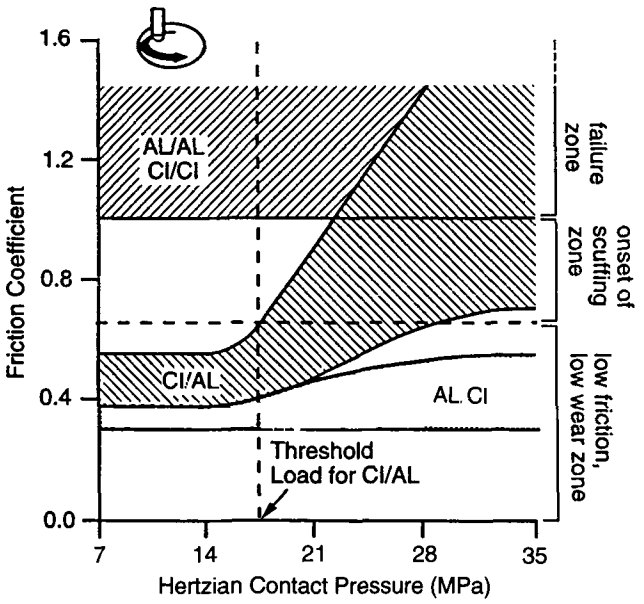

Fig. 3 Graph illustrating correlation between coefficient of friction and various modes of wear

which can be considered an area of "negligible improvement" if the surface-treated material falls within it.

The material's performance as tested with the pin-on-disk tribometer is depicted in Fig. 3, which classifies both Al/Al and cast iron on cast iron (CI/CI) as a "forbidden pair" which surely will scuff instantaneously at all value of Hertzian pressure in the range of 7 to 35 MPa (1020 to 5080 psi), in the absence of lubrication. It is interesting to note that the couple CI/Al fails at the threshold load of approximately 16.4 MPa (2380 psi) at the given test duration equal to 1500 cycles. Reversing the role of the members in friction, such that the aluminum alloy pin rides on a cast iron disk (stationary/moving or permanent contact/cyclical contact), leads to a different, presumably much higher, threshold load, which at a given duration of the test would define the onset of scuffing.

In conclusion, the threshold load criteria illustrated here become a function of the prospective application of the material system subjected to the test. Nevertheless, the proposed bench test clearly allows for quick detection of any improvement achieved with surface modification, by allowing simple comparison of coefficient of friction levels, critical threshold loads leading to the conversion of sliding friction into catastrophic failure, and time to failure. In this sense it is a very convenient tool for monitoring progress in surface modification.

One must realize that different pin-on-disk test assemblies would give different quantitative test results. In the presented case, hemispherical pin tips of 0.051 m (2 in.) radius were polished with 1 μm diamond paste. Disks were polished with 600-grit sand paper and, in the case of A390, subsequently etched to expose the primary silicon grains to provide better scuff resistance. Different surface preparations or some other routines not listed here might lead to different numerical results. Since dry sliding conditions using the pin-on-disk machine only approximate some real-world applications, by no means does this method provide sufficient information for the selection of materials for any real-world components. However, the described method seems to be an excellent tool for the initial screening of materials or determination of the quality of the material's surface modification, especially for applications where friction or scuffing under poor lubrication conditions is the major concern.

3.2 *Cameron-Plint Reciprocal Tribometer Test Procedure*

To enhance the chance for establishing a successful screening method, pin-on-disk tribometer findings were correlated with Cameron-Plint reciprocal tribometer results, which are traditionally used by the General Motors units engaged in tribological studies of automotive components. The tribometer provides a reciprocating motion between a moving sample and a stationary sample. It is possible to change the following conditions in the tribometer: stroke length, applied load, frequency of reciprocation, temperature, and lubrication conditions. For the experiments the following parameters were selected: constant load of 70 N, a stroke length of 9 mm, and a frequency corresponding to an average speed of 10.8 cm/s. Simulation of oil starvation, the factor responsible for the lack of lubrication, was a key element in our testing procedure and made possible the correlation of pin-on-disk results with the Cameron-Plint

tribometer tests. Following the existing standard procedure developed by others within the corporation, a quasi-lubricated condition to provide run-in and film formation was simulated by adding two drops of kerosene to the interface, which had been heated to 85 °C. The lubricant is then allowed to evaporate and decompose during the test, simulating a conversion to a

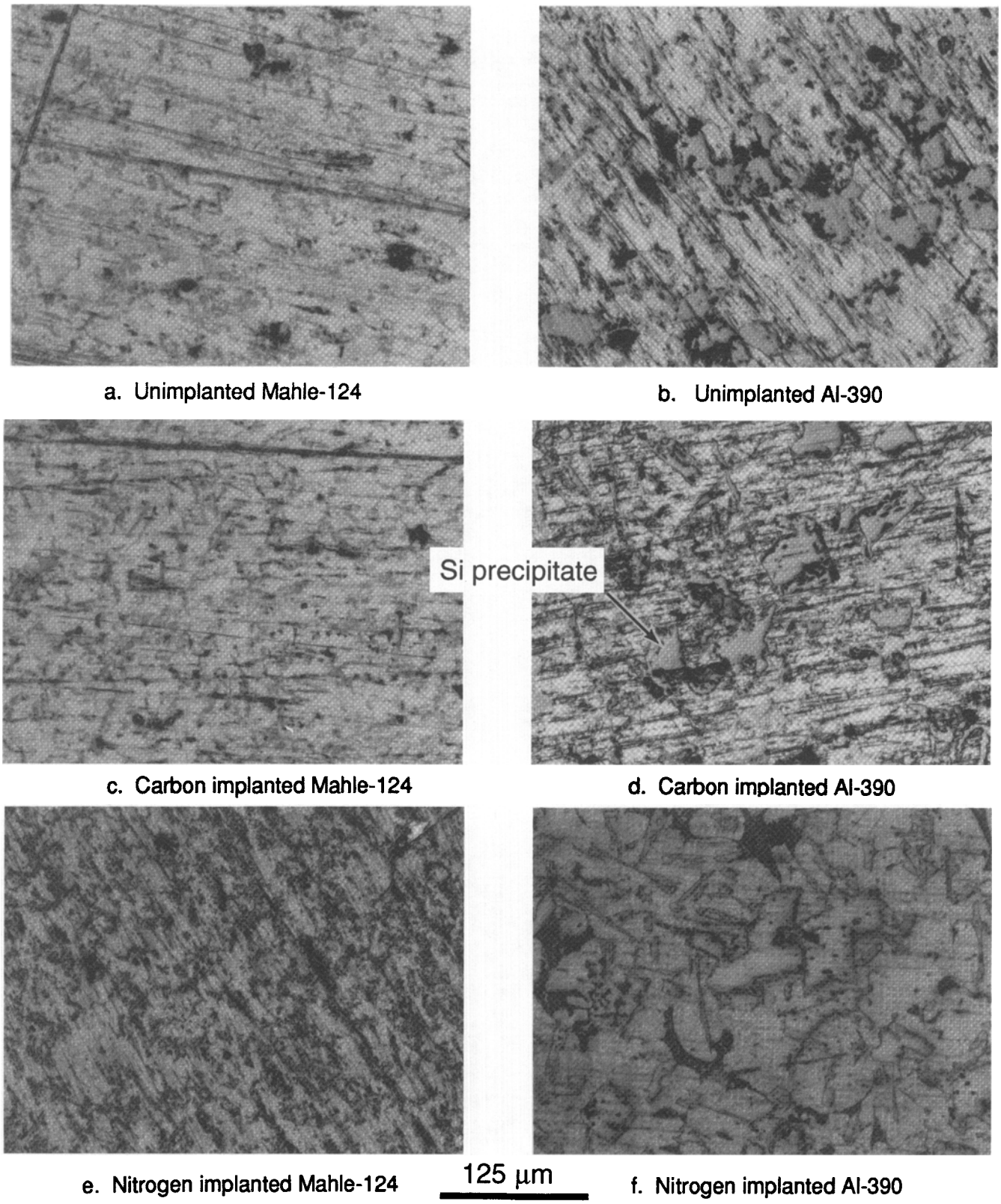

Fig. 4 Optical micrographs of the aluminum alloys before and after implantation. (a) Unimplanted Mahle-124. (b) Unimplanted A390. (c) Carbon-implanted Mahle-124. (d) Carbon-implanted A390. (e) Nitrogen-implanted Mahle-124. (f) Nitrogen-implanted A390

starved lubrication condition. Specifically, between 120 and 300 s the kerosene essentially evaporates, due to the interface elevated temperature and frictional heating. The test under oil-starved condition begins at that time.

Two factors are of importance in the evaluation of scuffing. One is the abrupt change in friction that presumably signals the onset of scuffing. To detect scuffing onset, a somewhat arbitrary criterion was applied which states that the rate of increase in the friction coefficient should be more than 0.2 in a 60 s interval. Secondly, to avoid extraneous events, it was determined that the value of the friction coefficient should be at least 0.35 for scuffing to occur. This defines the time to scuffing. Subsequently, a post-factum analysis of the samples validated the presence of material transfer, reflecting the presence of scuffing.

3.3 *Adhesion Test Procedure*

Whenever the surface treatment involves a deposition stage, it becomes important to supplement resistance-to-wear tests with an adhesion test, which quantifies bonding of an applied coating to a substrate.

The adhesion tests were performed on a Z-axis stud pull machine using Quad Group Inc. aluminum studs. The studs were delivered from the manufacturer, coated with an epoxy coating having a tensile strength of 80 to 100 MPa. These were mounted on the samples to be tested and placed in an oven to cure for 1 h at a temperature of 150 °C. They were then slowly cooled to room temperature. The studs were pulled away from the sample using the Z-axis stud pull machine. The pulling force that broke the bond was registered. For better statistics, six studs were mounted on each sample tested. The root-mean-square of the measurements was then calculated.

4. Surface Treatment Experiments

4.1 *Early Experiments ("Proof of Principle" Experiments)*

With the emphasis on modifying the surface properties of aluminum pistons, aluminum alloys A390 and Mahle-124 (composition close to that of aluminum alloy 336), both having

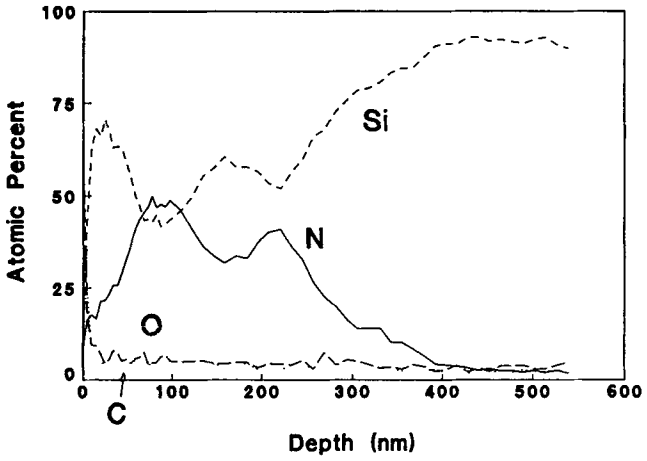

Fig. 5 Depth profile of the silicon phase of A390 implanted with nitrogen

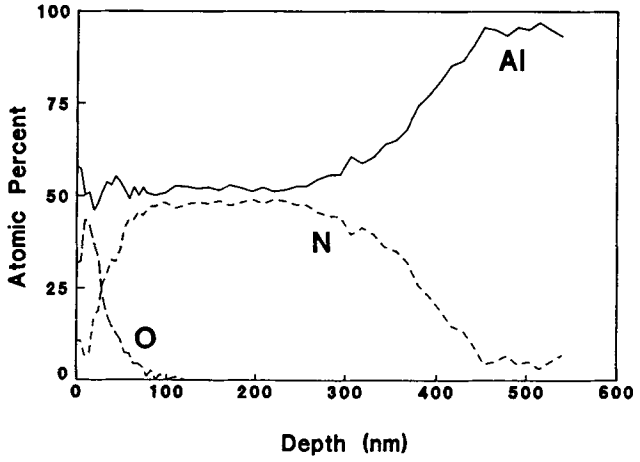

Fig. 6 Depth profile of the bulk phase of aluminum alloy A390 implanted with nitrogen

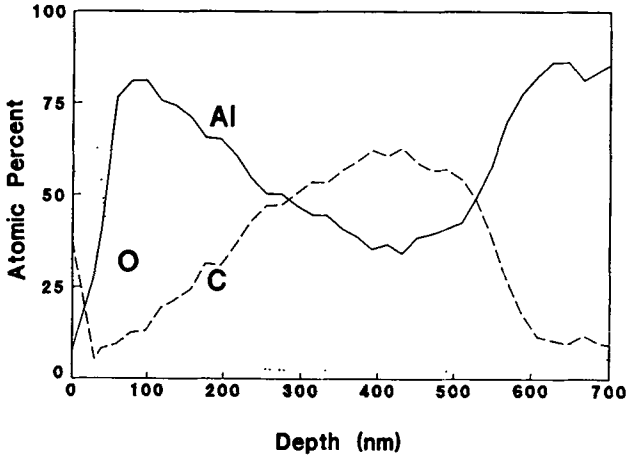

Fig. 7 Depth profile of the bulk phase of Mahle-124 (composition close to that of aluminum alloy 336) implanted with carbon

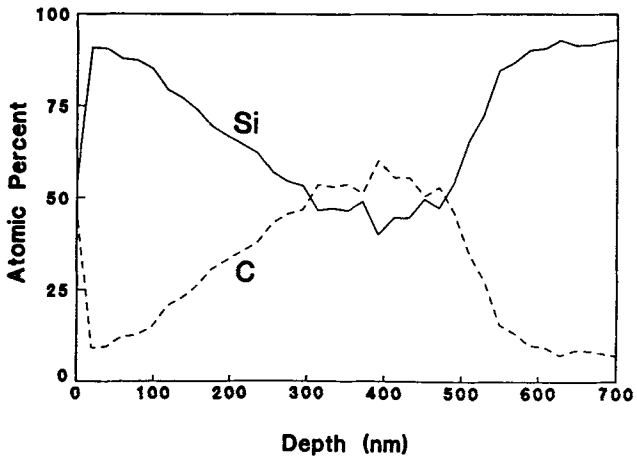

Fig. 8 Depth profile of the silicon phase of Mahle-124 implanted with carbon

a high silicon content, were chosen for most of the experiments. The goal was to verify whether ion implantation of carbon or nitrogen improves the wear resistance properties of the alloys. Since total dose and implantation energy seemed to be crucial for "proof of principle," implants were conducted with a well-controlled line-of-sight implanter. Nitrogen and carbon ion implants were performed at 100 keV to doses of 2×10^{17} and 1×10^{18} ions/cm^2. For the nitrogen implants, a Zymet Z100 implanter was used, which had no means of magnetically selecting ions. This resulted in the implantation of all possible nitrogen species from the source (atomic and molecular nitrogen with single or double charge). In the carbon implants the ions were magnetically selected to implant single ionized atomic carbon only. For that purpose a Varian/Extrion implanter was employed.

The as-prepared implanted surfaces were examined by optical microscopy and Auger electron spectroscopy (AES). AES was performed using a Physical Electronics model 600 scanning Auger microscope. Electron beam conditions of 5 kV and 0.03 μA yielded a probe diameter of less than 0.5 μm. Depth profiles were acquired using a differentially pumped argon ion gun. A 3 kV beam yielded a sputter rate of 49 nm/min on a tantalum pentoxide standard. Quantitation for nitrogen-implanted specimens was performed using sensitivity factors determined from bulk aluminum nitride (AlN) and silicon nitride (Si_3N_4) standards. Published sensitivity factors were used for quantitation of the carbon-implanted specimen. Micrographs were obtained using an Olympus model BH-2 light microscope. Micrographs were acquired using reflected light at magnifications of 200× and 500×. Figure 4 shows micrograph pictures for both aluminum alloys before and after implantation. Both alloys have silicon precipitates because the silicon contents are much greater than the solid solubility limit of silicon in aluminum (<1% Si). Differences in silicon content and trace elements may account for differences in silicon precipitate sizes. Due to the higher sputtering of aluminum the texture of the surface becomes more visible after implantation, especially in the case of alloy A390, which has 16 to 18% silicon compared to 11 to 12% for Mahle-124. A depth profile of a silicon precipitate in A390 implanted with nitrogen is shown in Fig. 5. A double Gaussian peak reflects the implantation of multiply charged atomic and molecular nitrogen ions. The first Gaussian peak is centered at approximately 90 nm and is due to singly ionized nitrogen (N^+). The tail which extends beyond 300 nm contains a second peak associated with the doubly ionized nitrogen (N^{++}). The Gaussian peaks maintain their shapes as a result of the low thermal diffusivity of nitrogen in silicon. On the other hand, the depth profile of aluminum matrix does not show the double peak feature because of the high thermal diffusion of nitrogen in aluminum (see Fig. 6). The concentration of implanted nitrogen into aluminum does not exceed the stoichiometric ratio of 1:1 for AlN, which is consistent with other observations (see Ref 12).

Figure 7 displays the depth profile of the aluminum matrix in Mahle-124 implanted with carbon. The concentration of carbon exceeds the stoichiometric ratio of aluminum carbide, Al_4C_3. This suggests the possibility of carbon segregation in aluminum. The compositional ratio of silicon to carbon inside a silicon grain of the same sample (Fig. 8) is slightly higher than one. This confirms reports by others (see Ref 13) that carbon atoms tend to form clusters inside silicon.

Sliding wear resistance tests were performed, at this early stage of research, on a computer-driven Faville-LeVally Falex Block-on-Ring wear tester (Fig. 9a). The tester and adopted screening routine, which is summarized below, were a common standard for screening tribological behaviors of bulk materials. Wear test results are summarized in Table 1. Generally, ion-implanted samples showed improved wear resistance compared to unimplanted alloys. The poor correlation between subsequent runs of similar samples is an indicator of the low reliability of this testing method. This routine was not designed for testing materials with tribological properties modified at the very surface, i.e., to a depth measured in only a fraction of a micrometer. The test was run at a constant load of 20 MPa with the ring rotating at 500 rpm for 2 h or until the wear depth was 50 μm, whichever was attained first.

The real difference in the wear rate occurred during the first few minutes, before the block broke through the modified (implanted) layer. Later, the wear reflected the property of the bulk material and became irrelevant for the experiment. Uncertainty of the test results was further increased by the fact that the initial contact area between the block and ring was unknown and varied from sample to sample. Attempts to seat block-ring sets by running-in prior to the implantation (see Fig. 9b) were unsuccessful. This was due to variation in the contact pressure during the initial break-in period, making the whole procedure questionable unless the total testing time is much longer than the initial running-in period, which is not the case if a material surface property is altered on a submicron scale. These difficulties thus prompted us to seek a different diagnostic tool suitable for the assessment of the near-surface tribological improvements resulting from the PIII treatment. This led us to the pin-on-disk bench test standard.

4.2 *Friction and Resistance to Wear of Ion-Implanted Aluminum Alloys*

Modification of a material is typically limited to the subsurface region, measured in hundreds of angstroms only. Consequently, if a high load is applied to the surface such that it causes the stress fields to penetrate deep into the bulk of the otherwise soft material, surface modification by ion implantation becomes virtually useless. Application is questionable also when persistent friction, despite improved resistance to wear,

Table 1 Results of the sliding wear resistance test

Implant species	Time to failure(a), min
Mahle-124	
Unimplanted both sides	10, 15
Nitrogen	26, 18, 64, 114
Carbon	532, 103
A390	
Unimplanted both sides	123, 158
Nitrogen	250, 1154, 4930
Carbon	322, 2838

(a) Failure was considered to have occurred when a wear depth of 50 μm (0.002 in.) was attained.

wears the surface beyond the modified area before the end of the expected life of a component. Therefore, when application is limited to the surface improvement of automotive components, ion implantation may be severely restricted in its potential applications, unless it is combined with other vacuum-based techniques allowing for surface alteration on the order of microns rather than submicrons.

Consequently, this paper documents only some basic tribological characteristics of nitrogen-implanted A390 alloy, for the sake of creating a reference base for further experiments where ion implantation is combined with other surface treatments.

In order to maintain well-defined implantation conditions while creating this reference base, the treatment was performed with a well-controlled line-of-sight implanter at 100 keV and at two different doses: 5×10^{16} and 1×10^{17} ions/cm^2. Friction of the modified A390 samples was tested with a pin-on-disk tribometer and compared to the performance of the nontreated base material. The experimental routine consisted of running untreated A390 pins against treated A390 disks without any lubrication. Tests were repeated for three different contact pressures (10, 13, and 15 MPa), defined by selected loads (5, 10, and 15 g) applied to the system and various pin curvatures.

In general, nitrogen-implanted aluminum showed a reduced coefficient of friction when compared to the untreated material (Fig. 10). Comparison of two different implantation doses (Fig. 11) indicates a difference in performance during the early stage of the wear process (each graph has two curves, indicating two identically treated samples). This difference becomes a statistical variation once the wear breaks through the modified layer and the performance curves of the two converge. The initial difference in the coefficient of friction and the convergence toward the behavior of the base material for the two different doses may be attributed to different abrasiveness and different brittleness of the treated A390, respectively.

Despite this improvement, since the surface is modified only on a submicron scale (see Fig. 5 and 6), progressive wear eventually narrows the difference in performance of the treated and untreated samples, which can be clearly demonstrated by changing the time scale of the pin-on-disk experiment (see Fig. 12). This result obviously confirms our pessimistic assessment of the limited attractiveness of ion implantation for automotive components, which typically require a long service time. In conclusion, effective improvement of aluminum alloy components most likely cannot be achieved with ion implantation

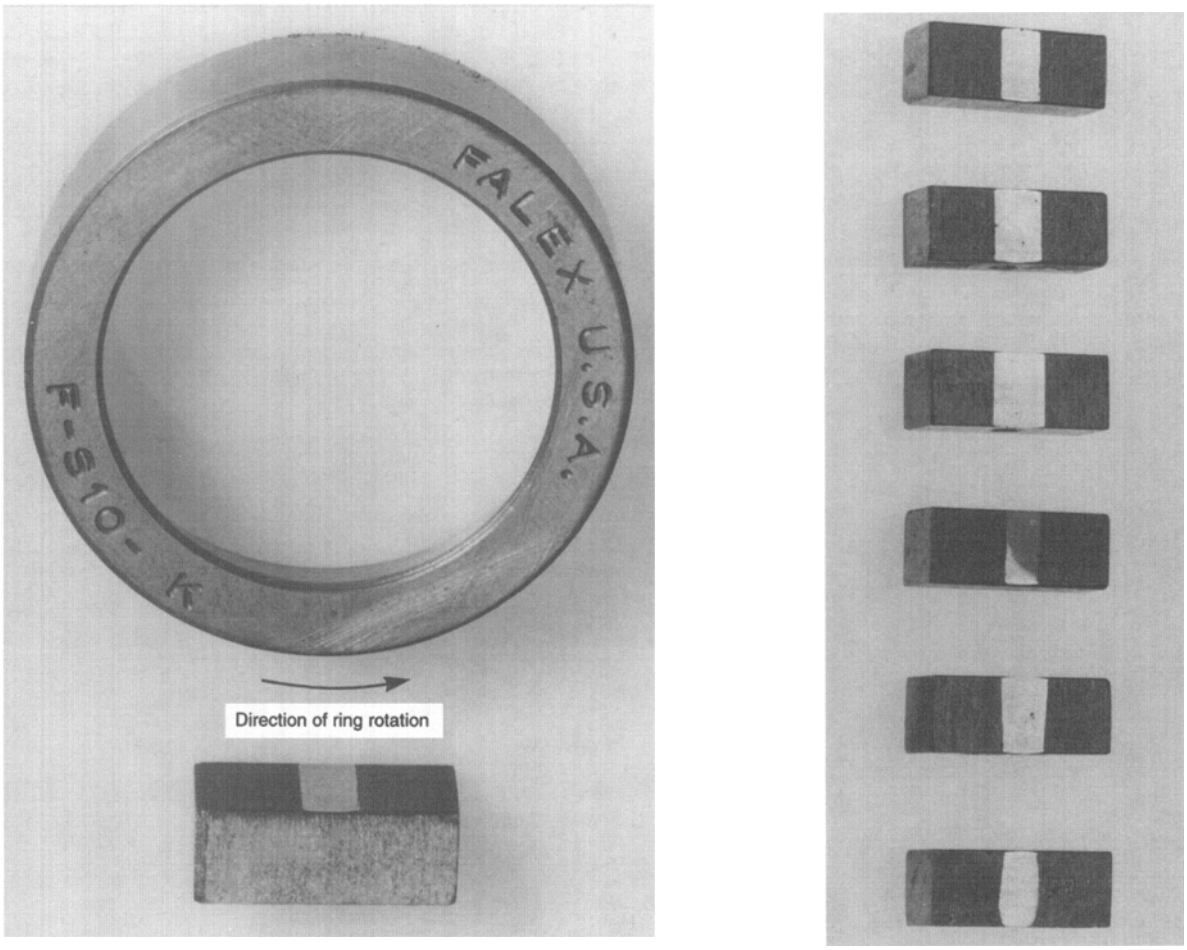

(a) (b)

Fig. 9 (a) Faville-LeVally wear tester elements: the system's ring and block (magnified). (b) Samples which were wear tested under the same conditions. The difference in the width of the scars indicates the improper contact due to improper seating in spite of the preseating procedure. 4×

alone, and hybrid surface treatment methods must therefore be considered.

4.3 *Diamond-like Hydrocarbon Coatings*

In the majority of automotive applications, as described above, surface modification on a submicron scale seems to be insufficient, regardless of the achieved improvement. Even a low friction surface, in a persistent wear environment, will wear out the toughest modified layer unless its thickness is sufficient to survive past the component's life, which may be measured in tens of years. Therefore it is long-term wear that defines the system durability, mostly in the presence of gradually deteriorating lubricant which occasionally overloads the surface, requiring that it survive under a lubricant-starved condition. It is believed that a high-quality surface-modified layer on the order of a few microns may be suitable for such applications.

Because of its unique combination of good chemical inertness, low friction, and high wear resistance, diamond-like hydrocarbon coatings (DLHC) are good candidates for coating of some automotive components, particularly where elements are subjected to limited lubrication or where high wear is of concern. DLHCs can be prepared by a wide variety of methods (see Ref 14), including processes using a plasma reactor with a hydrocarbon gas source, a technique similar in its principle to PIII.

As with any metallurgical coating, adhesion between the substrate and the coating is critical to the success of the application. Adherent DLHC have been deposited successfully onto nonferrous metals (Ref 15) and steels (Ref 16). In particular, high film adhesion was achieved on a 6061-T6 aluminum substrate with the prior removal of surface oxides by employing argon sputtering (Ref 17). Both oxide removal and the subsequent surface preconditioning in the form of a mating amorphous-silicon-hydrocarbon interlayer (Ref 17) have been proven to be crucial in the formation of a strong bond between DLHC and the metal substrate.

The interest of the automotive industry in high-silicon-content aluminum alloys (pistons and engine blocks) creates some limitations in the selection of suitable surface coating materials. When considering A390, for example, the processing tem-

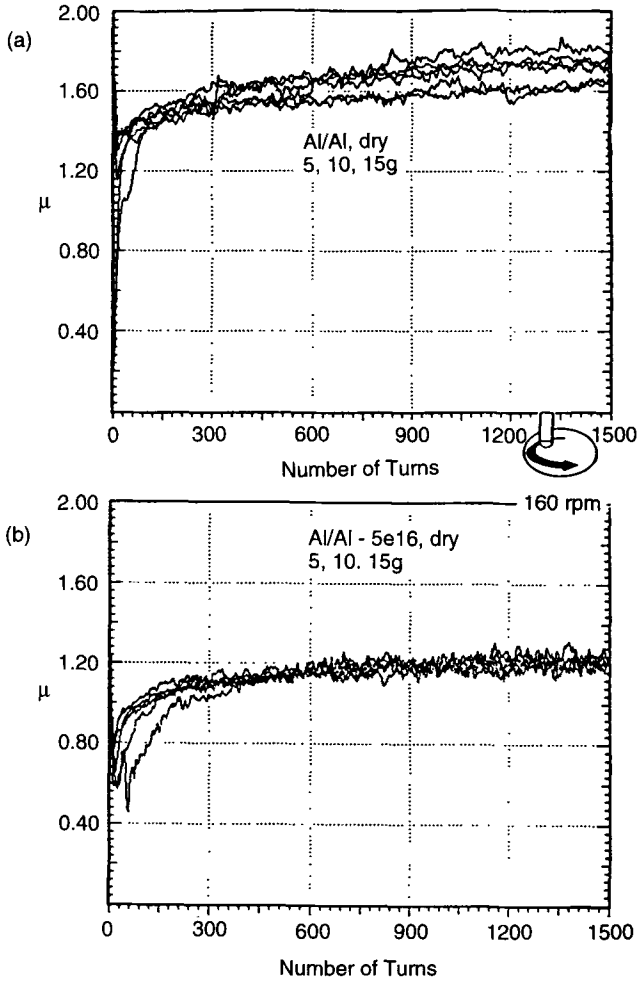

Fig. 10 Pin-on-disk test results for three different contact pressures and two different linear speeds of the pin. (a) The untreated A390/A390 pair. (b) A390 pin running against A390 disk implanted with nitrogen (dose 5×10^{16} cm^{-2})

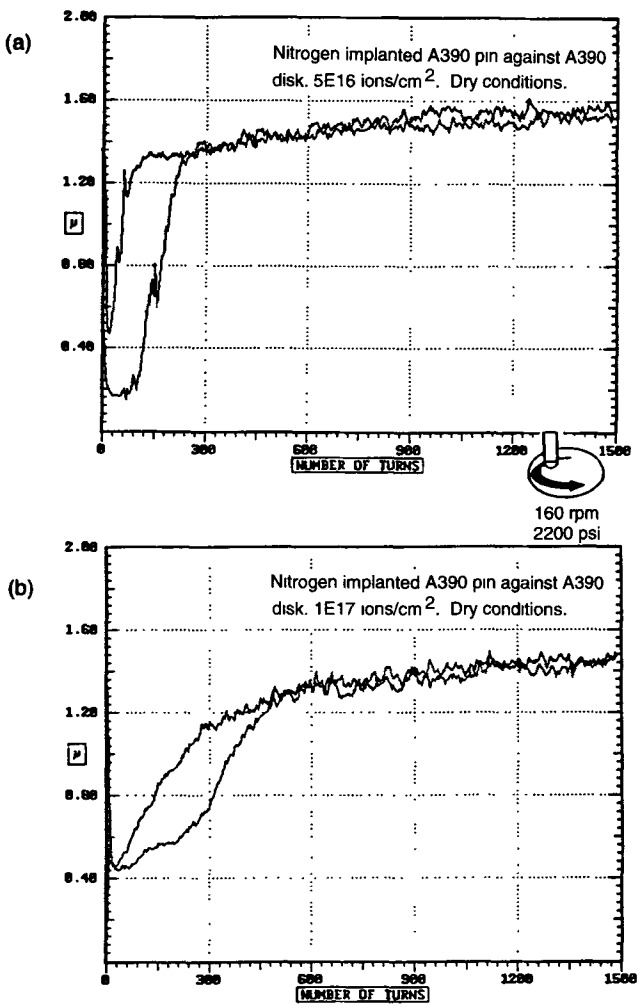

Fig. 11 Coefficient of friction test results for two different implantation doses into A390 pin run against unimplanted disk. (a) Nitrogen dose 5×10^{16} cm^{-2}. (b) Nitrogen dose 1×10^{17} cm^{-2}

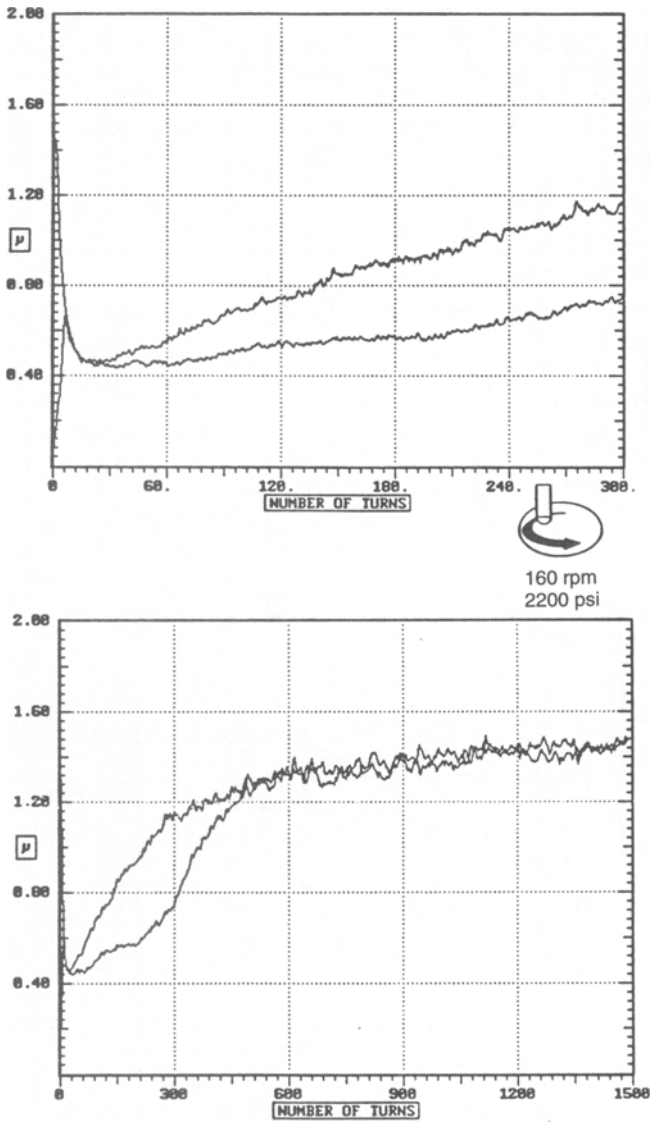

Fig. 12 Pin-on-disk test results for two different total number of revolutions, indicating the wear of the implanted layer (nitrogen implantation dose 1×10^{17} cm^{-2})

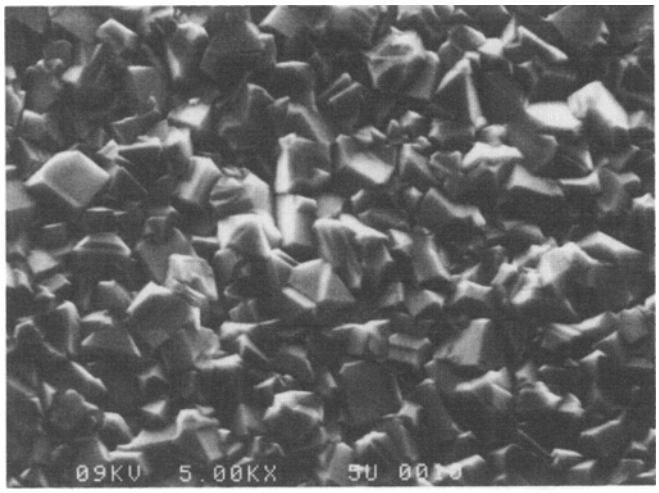

(a)

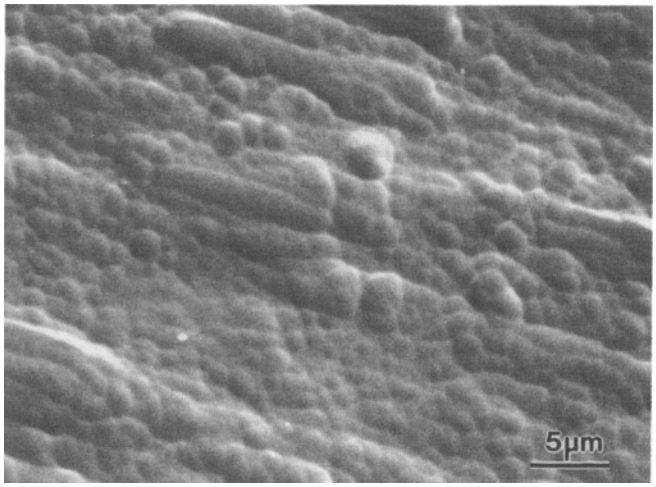

(b)

Fig. 13 (a) Typical morphology of diamond films. (b) Morphology of the DLHC made by the acetylene plasma beam technique

perature must be kept below 220 °C in order that the alloy does not lose its original metallurgical properties. In addition, an oxide layer, which always grows on the surface of the aluminum alloy, is difficult to remove. Accounting for these limitations, a one-stage vacuum operation consisting of oxide removal, interlayer build-up, and subsequent DLHC, all run in the PIII mode, seems to be an attractive choice for surface treatment of A390.

In order to create a reference base which would allow the evaluation of the quality of PIII-grown DLHC, several samples of A390 were treated at Colorado State University, using the line-of-sight coating procedure developed there by P.J. Wilbur and his associates (Ref 17-19). Briefly, the method consists of ultrasonic cleaning sequentially in three different solvents. Later, a Si:C bond interlayer, several angstroms thick, was deposited on the freshly argon sputter-cleaned surface and a DLHC was deposited as the final coating. The interface Si:C layer, about 50 nm thick, is sputter deposited by bombarding a silicon target with argon in a backfill of methane gas. The DLHC is formed by acetylene plasma beam accelerated to about 450 eV.

DLHC feature a smooth surface that differs from the morphology of most diamond films, which typically are represented by a more abrasive surface (Fig. 13). Lower abrasiveness of the film selected for our experiments becomes a major issue of relevance for applications different from cutting tools, i.e., for systems where long-term resistance to wear and low friction are crucial for proper functioning and survival.

Despite these attractive tribological behaviors, DLHC cannot be considered for applications in the automotive industry unless it is demonstrated that the deposition procedure allows for mass production of parts, together with a reasonable capital investment and operational costs. If the DLHC formulation

were limited solely to batch processing offered by PIII, the manufacturing problems could be addressed and DLHC would be feasible for mass production.

The uniqueness of aluminum alloys which include silicon grains seems to create the opportunity for PIII-based growing of DLHC. It may be hypothesized that the bond interlayer in the form of Si:C can be created by carbon implantation onto silicon grains, or at least that the implantation of carbon into high-silicon A390 alloy provides an equivalent bonding surface as the Si:C bond layer. At the same time, it is expected that the carbon bombardment of the aluminum matrix results in aluminum carbide formation and thus limits oxygen reentry onto the surface of the alloy. In short, it is anticipated that argon sputter cleaning plus subsequent carbon implantation provides sufficient surface preconditioning to promote adhesion of the DLHC to the aluminum alloy substrate.

Initial experiments with the above-formulated sequence of surface treatments using PIII processing showed partial flaking and delamination of the coatings. The experiment was repeated with different substrates, not necessarily aluminum alloys, with similar results. In order to identify the source of the poor adhesion of the DLHC, surface analyses of the samples were performed after each step of the three-step process for both the Colorado State and the IONCLAD processes. At each step, x-ray photoelectron spectroscopy (XPS), AES, transmission electron microscopy (TEM), and x-ray diffraction (XRD) were performed. The back surfaces of some of the samples were also analyzed to determine a baseline reference for contaminant elements.

Identification of the cause of the poor adhesion was found while examining differences after the second step of the processing sequence, the one designed to create the bonding interlayer (Ref 20). Specifically, TEM and XRD analyses showed no evidence of crystalline formation of silicon carbide for either case, the line-of-sight sputtering of silicon with argon with the methane backfilling, or the carbon implantation from methane plasma run in IONCLAD mode.

The PIII-treated sample featured amorphous carbon, detected by TEM and confirmed by AES. This amorphous carbon layer is responsible for the delamination of the final DLHC processed following the PIII technique.

The mechanism for the formation of the undesired amorphous carbon layer is an intrinsic outcome of the PIII technique. Clearly, any train of negative pulses applied to the target features a finite rise and fall time of the individual pulses, due to the dynamically changing electric load conditions and limitations in the design of the pulser. When implanting with such a pulse shape, the accelerated ions will have a spectrum of kinetic energies upon impact. At lower energies, less than 1 keV, the accelerated ions subtracted from the methane plasma will be deposited as a carbon film at the surface instead of being implanted. As the individual pulse progresses, ion energies increase and implantation occurs. With time, the carbon deposition continues, but the higher-energy ions, representing the plateau of the pulse, penetrate and damage this film. The film build-up is, to some extent, limited by self-sputtering.

Thus, an amorphous carbon layer of limited thickness is created together with the desirable carbon implant. The ratio of these resultant carbon forms depends on pulse shape and peak

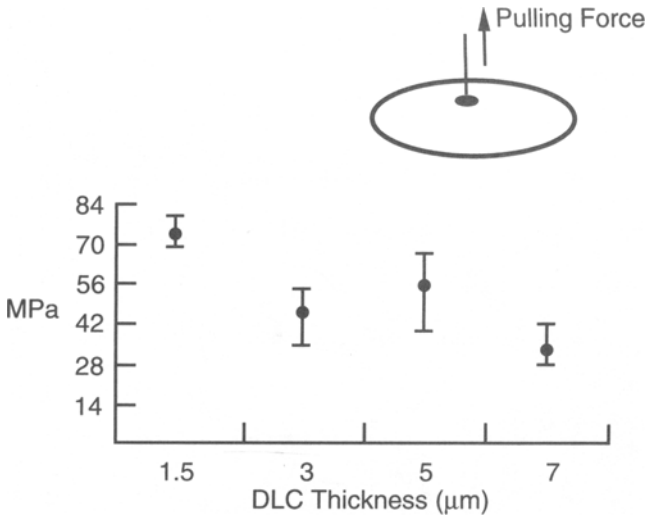

Fig. 14 The pulling force resulting in the stud separation from the DLHC as a function of the film thickness

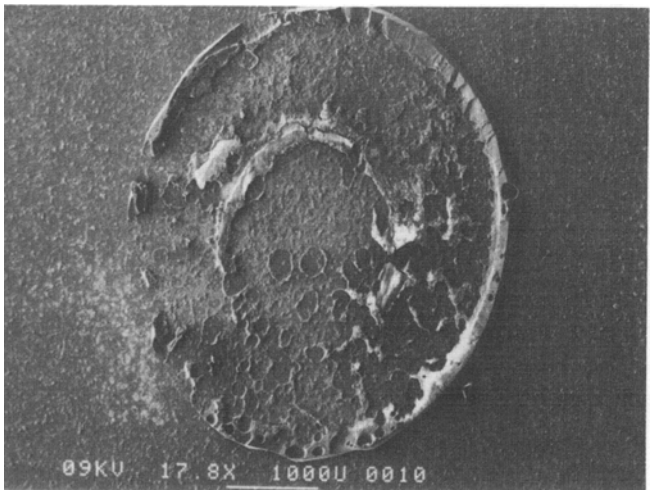

Fig. 15 SEM micrograph of an adhesion-tested sample coated with a 5 μm DLHC

pulse amplitude, i.e., it depends on the kinetic energy spectrum of the involved carbon ions upon impact with the target. It is also anticipated that during the off-period between pulses, neutral carbon or other contaminants may be deposited from the plasma and contribute to the build-up of an amorphous carbon layer.

To remove the unwanted amorphous carbon layer without affecting the implant, a limited argon sputter-cleaning was introduced, which wipes out the contaminant before the DLHC step is started. Surface analysis performed on sputtered bonding layers indicated the effective removal of excessive carbon from the surface. Subsequently, DLHC deposited onto the sputter-cleaned adhesion interlayer showed no signs of flaking or delamination, and adhesion measurements demonstrated a bond quality equal to that achieved with the line-of-sight formula.

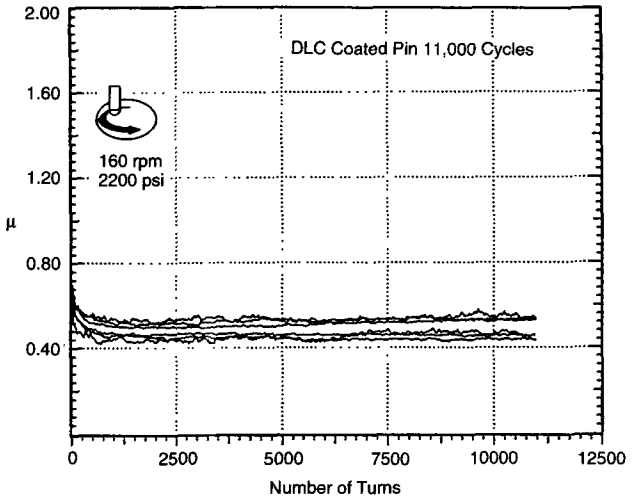

Fig. 16 Friction coefficient for a DLHC-coated pin running against a bare A390 disk

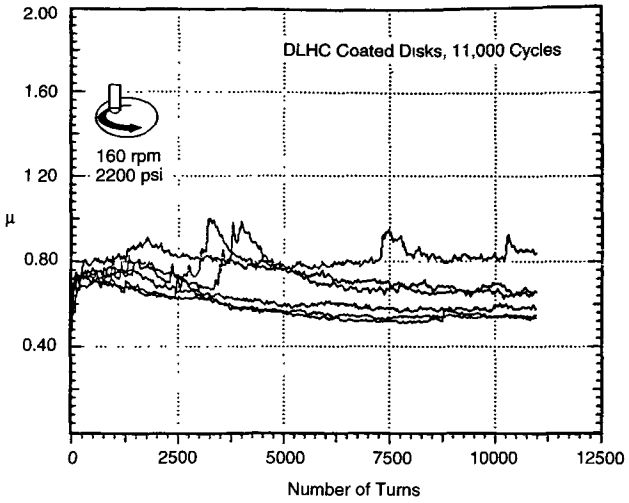

Fig. 17 Friction coefficient for a DLHC-coated disk running against a bare A390 pin

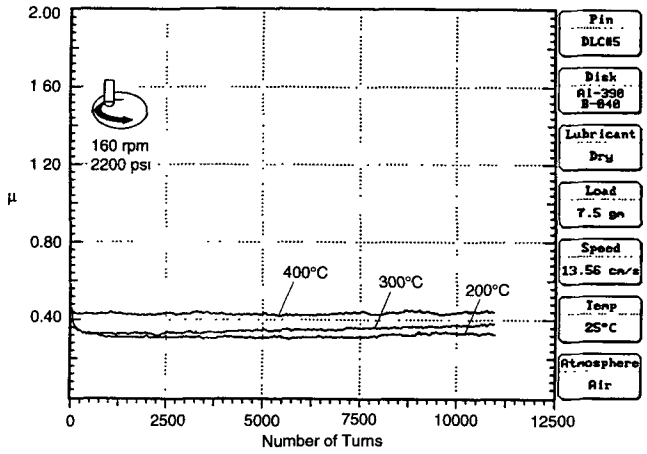

Fig. 18 Friction coefficient for a DLHC-coated and thermally cycled pin running against a bare A390 disk

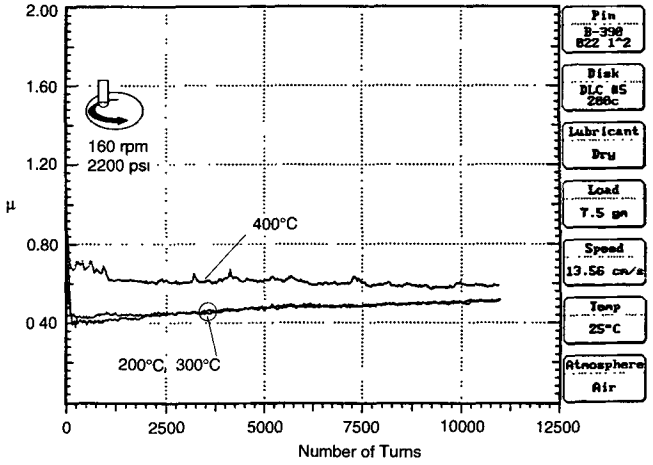

Fig. 19 Friction coefficient for a DLHC-coated and thermally cycled disk running against a bare A390 disk

5. Tribological Characterization of DLHC on A390

The wear and adhesive properties of DLHC-coated alloy A390 have been evaluated. Tests were performed with several different coating thicknesses, ranging between 1.5 and 7 μm.

Adhesion measurements, performed following the test procedure described in section 3, indicate that in general the pulling force decreases with the increase of the coating thickness (see Fig. 14). However, visual inspection of the studs and the marks left on the samples indicate that for the lower thicknesses (1.5 and 3 μm), the film is almost completely removed, uncovering the A390 substrate. For the thicker films (5 and 7 μm), however, the separation took place at the interface of the epoxy and the DLHC rather than at the interface of the DLHC and the A390 substrate. The latter result is clearly visible in Fig. 15, which shows an SEM micrograph of an adhesion-tested sample that had a 5 μm DLHC. Thus, it appears that the adhesion of the thicker DLHC is equal to or higher than that registered by the stud-pull machine. In conclusion, further investigation is required, which will include both adhesion and cohesion of the DLHC.

The pin-on-disk bench test procedure requires that during an unlubricated test (dry surfaces) the friction coefficient must remain below 0.8 for a Herzian contact pressure of 17.25 MPa for a minimum of 1500 cycles. DLHC-coated A390 pins were run against bare A390 disks, and bare A390 pins were run against DLHC coated A390 disks. The results of the measured coefficient of friction versus number of cycles are shown in Fig. 16 and 17, respectively. For the DLHC-coated pin on the bare A390 disk (Fig. 16), the value of coefficient of friction is less than 0.6 throughout the duration of the test for each of three different pressures (12.5, 15.2, and 17.25 MPa) for a test duration much longer than required (11,000 cycles vs. required 1500). For the A390 bare pins run against DLHC-coated disks (Fig. 17), only after 2,500 cycles did some of the samples exceed the predefined critical value of 0.8, for the coefficient of friction. In both cases, the performance of the DLHC coating was superior to that of the base materials tested earlier (Fig. 3).

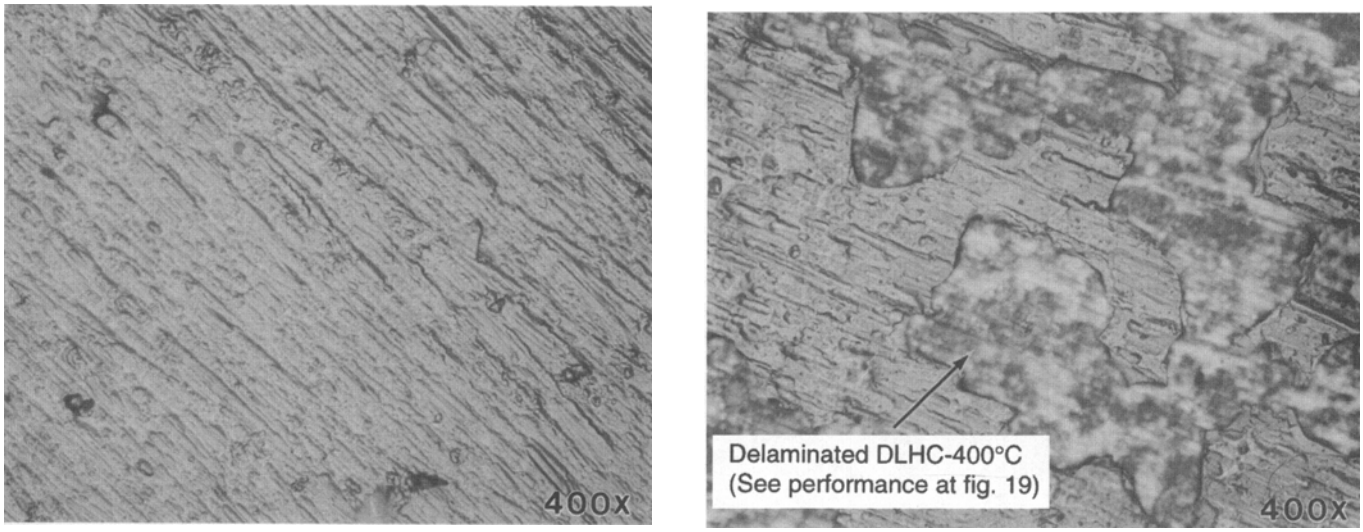

(a) (b)

Fig. 20 (a) Micrograph of an as-deposited DLHC. (b) Micrograph of a thermally cycled DLHC at 400 °C (arithmetic mean roughness value of the original surface was 0.12 μm)

Requirements of automotive applications demand that components survive thermal cycling. The results of the friction measurements of the DLHC/thermally cycled pin or disk are shown in Fig. 18 and 19 for the three peak temperature settings of 200, 300, and 400 °C. The highest friction coefficient was experienced for the sample thermally cycled up to 400 °C. Nevertheless, for all temperatures, the DLHC exhibited excellent performance for the duration of 11,000 cycles, with the friction coefficient being around 0.4, about 50% lower than the threshold level where scuffing is initiated on the bench test.

Micrographs of the as-deposited DLHC and the worst performing thermally cycled DLHC (400 °C) are shown in Fig. 20. It is evident that the thermally cycled DLHC contains surface pits. This is due to either local decomposition or flaking of the coating. Despite this surface damage, this sample had a low friction coefficient when run against bare A390.

It is widely accepted that there is no single laboratory testing routine which, with a high degree of confidence, is able to assess the tribological performance of any system exposed to friction and wear. A variety of bench tests, if results correlate well, are indicative of system behavior in a real application. For this reason, the Cameron-Plint reciprocal tribometer was also used to verify findings obtained from the pin-on-disk experiment. Reciprocal movement and simulation of lubricant-starved test conditions differ from those experienced when employing the pin-on-disk machine, broadening the variety of conditions the tested system was exposed to.

It was found, when employing the reciprocal tribometer, that the thicker the DLHC, the longer the time before the couple fails, i.e., scuffing occurs (Fig. 21). This can be interpreted as a measure of the time to the wear-through of the coating. The variation of time to failure for samples of the same DLHC thickness results from variation in the contact area between moving and stationary members of the tested couple; the effect of such misalignment is an increase in the contact load. Differences in wear of 7 μm thick DLHC against bare A390 at a load of 70 N for conformal contact and point contact are illustrated

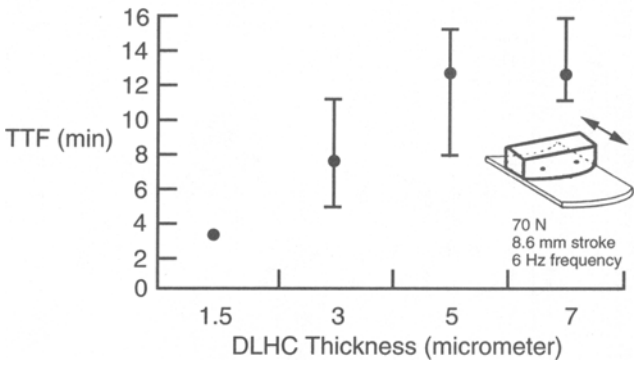

Fig. 21 Time to failure of DLHC as a function of thickness at a load of 70 N

in Fig. 22. The corresponding friction measurement results shown in Fig. 23 clearly indicate the radically different times to failure, which are clearly due to the preciseness of the couple conformality. Tests performed on the untreated cast iron/aluminum 390 couple, a proven good performer (current piston/liner couples in automotive combustion engines), indicate that the performance of the DLHC falls within the range of other well-performing material couples (Fig. 24).

6. Prospects for Improving Automotive Power Train Components

Power train components, whether or not operating in a lubricant-starved environment, experience gradual wear, leading to excessive noise, vibration, and ultimately functional failure. Therefore, formation of hard, lubricious films on structural substrates might result in substantial improvement of the overall performance of an automobile. Clearly, for example, any improvement in the performance of a piston-bore assembly is critical and would be a milestone in automotive technological development.

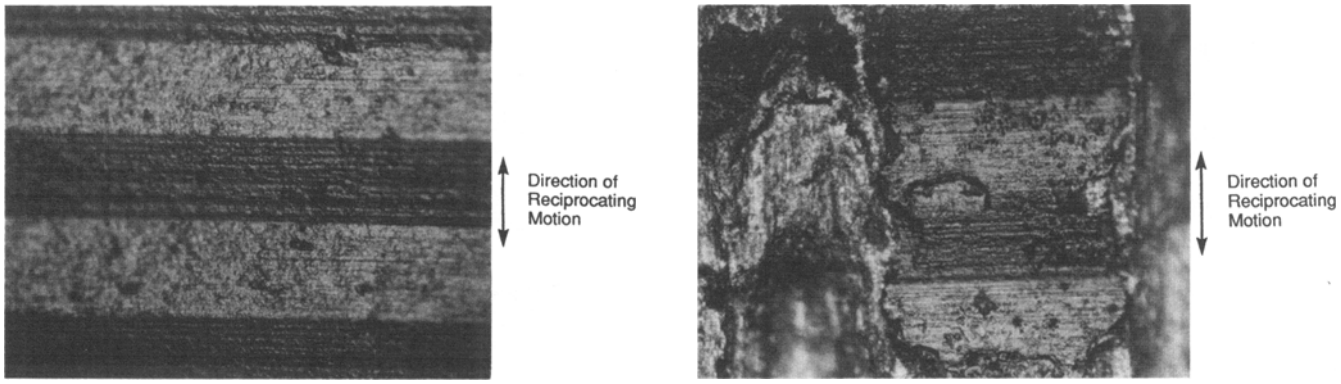

(a) (b)

Fig. 22 Wear surface of 7 μm thick DLHC against A390 at a load of 70 N. (a) Conformal contact. (b) Point contact

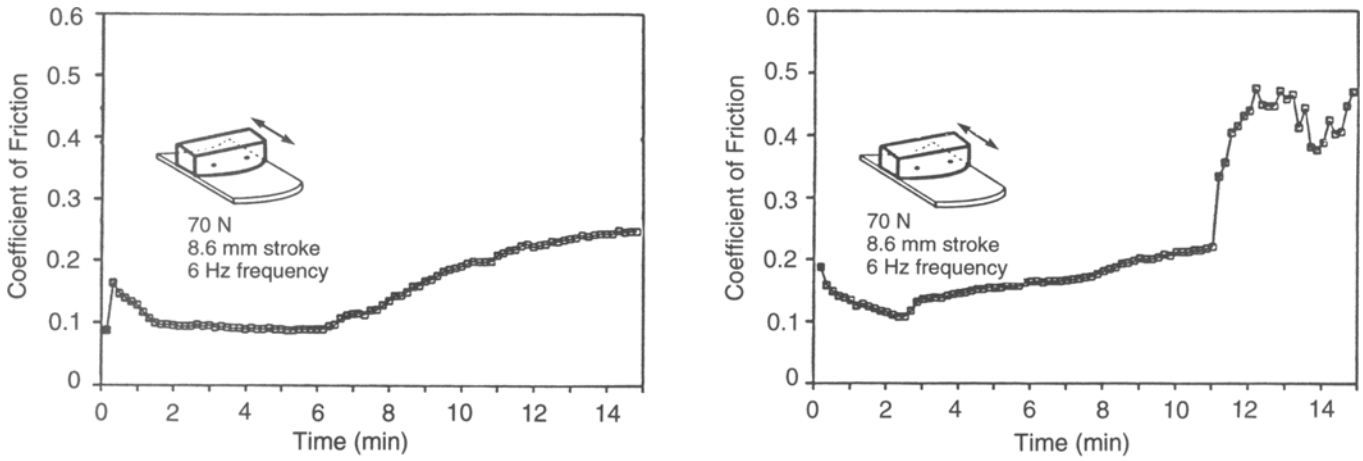

(a) (b)

Fig. 23 Cameron-Plint reciprocal tribometer measurements of the friction coefficient of a 7 μm thick DLHC against bare A390 at a load of 70 N. (a) Conformal contact. (b) Point contact

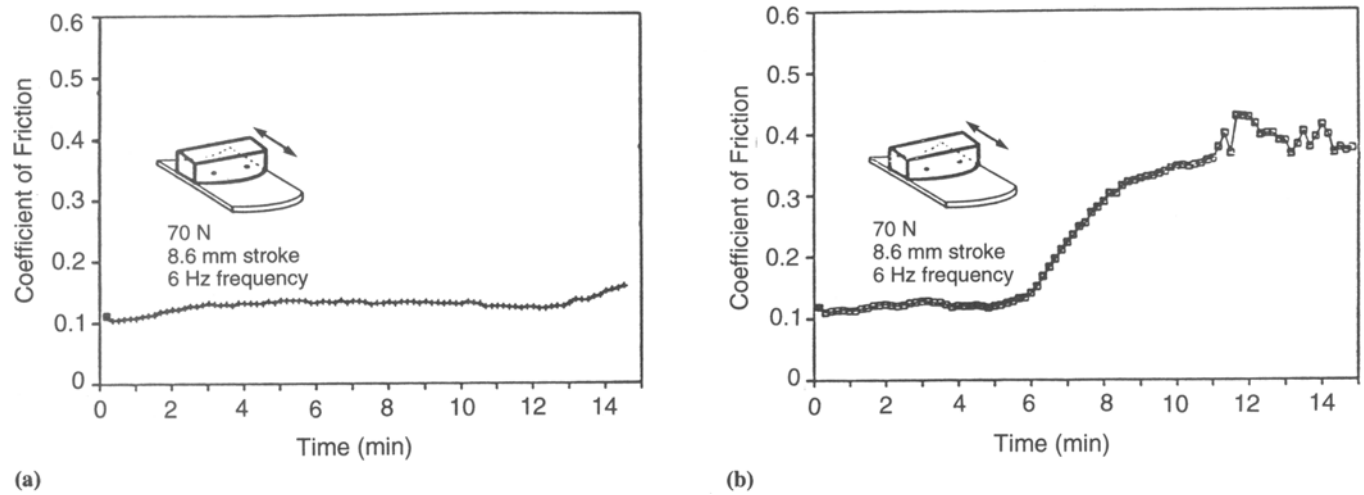

(a) (b)

Fig. 24 Cameron-Plint reciprocal tribometer measurements of the friction coefficient of the section of iron-plated piston against bare A390 at a load of 70 N. (a) Conformal contact. (b) Point contact

The current aluminum piston-bore technology utilizes, in most cases, cast iron liners in the bores of aluminum alloy engine blocks. The disadvantages of this system are high cost, increased weight, thermal expansion mismatch between the liner and the bore, and reduced packaging flexibility. An alternative technology involves iron plating of the aluminum piston surface, which allows for the engine block to be made entirely of an aluminum alloy. The traditional iron plating processes, however, make use of cyanides which are not easily disposed of and, therefore, face total elimination due to environmental restrictions. New technologies for iron plating are being developed to address toxicity and coating uniformity.

Still another approach in resolving the piston-bore scuffing problem is to modify either the piston skirt or the bore surface. The DLHC falls into this category and, in the light of the integrated, all-vacuum IONCLAD-based technique, is a quite promising option for improving the manufacture of all-aluminum combustion engines. From this perspective, our aim was to demonstrate that a suitable coating for aluminum pistons would allow the elimination of iron liners from aluminum block engines.

Initial screening of DLHC-coated aluminum alloy was performed by comparison of pin-on-disk test results of the treated samples with those of an aluminum alloy/cast iron couple (Al/CI). Comparison of the friction coefficient for both couples indicates the superior performance of DLHC-coated samples in the whole range of selected contact pressures (Fig. 25), at least when tribological properties were screened with a pin-on-disk machine. Subsequently, the Cameron-Plint reciprocal test was performed. The DLHC-coated section of an aluminum piston running against a section of specially casted bore, made of the same aluminum alloy, was compared with samples taken from a current engine employing specially made bare aluminum alloy bores and aluminum alloy iron-plated pistons. The test was limited to 5 μm thick DLHC which restricts the system's time to failure representing the total wear of the coating. Despite this limitation, results for the DLHC indicated that DLHCs are serious competition for iron plating technology (compare Fig. 26).

Tribological tests run either in dry conditions or when the tested systems are subjected to wear simulate some very specific service conditions not experienced during most of the life of an automobile. For most of the engine life, proper lubrication and the action of the piston rings limit the contact between the piston and the bore. The lubricant film prevents physical contact, so material transfer does not occur. This effect can be demonstrated by running a set of identical materials in the presence of lubricating film. Neither the pin-on-disk nor the Cameron-Plint reciprocator is able to distinguish differences between tested materials until the lubricating film breaks and physical contact is experienced. Such severe conditions may or may not occur during the life of an automobile. Nevertheless, the system must be able to survive it, as the material transfer is a cata-

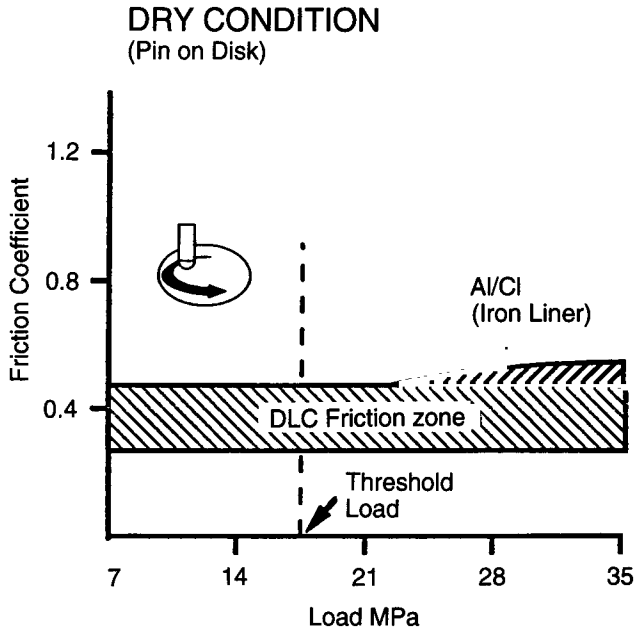

Fig. 25 Comparison of the friction coefficient for Al/Al, Al/CI and DLHC/Al couples as a function of contact pressure (pin-on-disk tribometer results; 11,000 cycles)

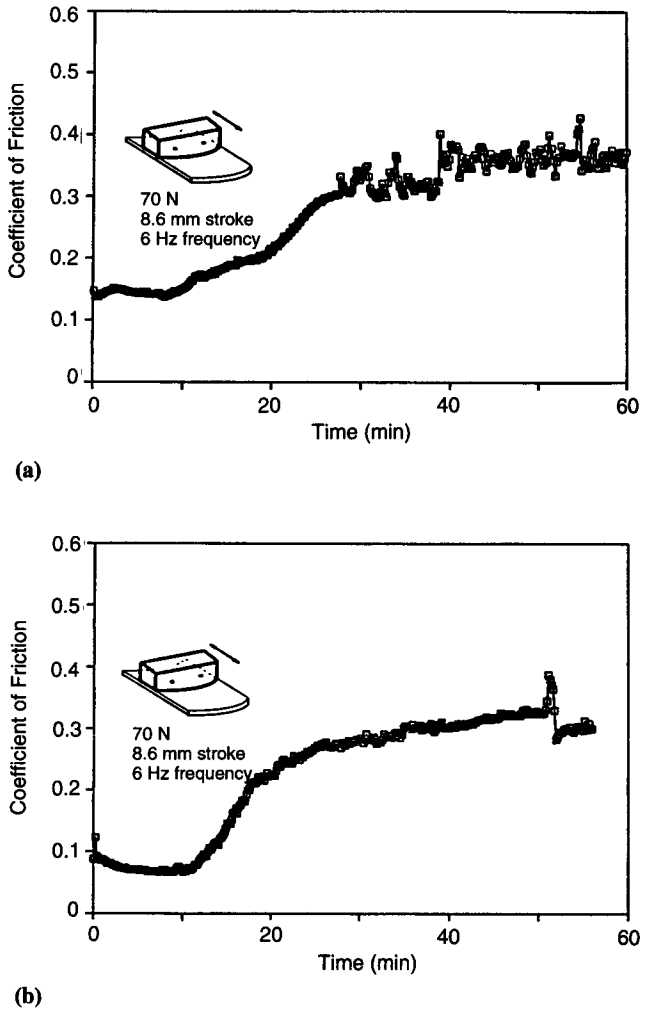

Fig. 26 Cameron-Plint test results showing the coefficient of friction curves for (a) iron-plated aluminum alloy piston section on A390 and (b) 5 μm DLHC-coated A390 piston on the bare A390 section of the bore. Run was performed under standard semidry conditions at a load of 70 N.

strophic event for the combustion engine. For example, cold scuff conditions may be generated when an engine, being out of service for a prolonged period of time, is started when the ambient temperature is low, such that the delivery of the lubricant is delayed due to its high viscosity. Therefore, the field testing for cold scuff is not a trivial issue and relies on a battery of tests which are expensive and time consuming.

Subsequent to the reciprocal tribometer test, the 1.5 μm DLHC-coated A390 pistons were tested in an engine dynamometer stand where they were run against custom-made bare A390 bores. In our engine dynamometer test procedure, which is a part of the cold scuff test, the engine water pump was connected directly to the servicing chiller. Coolant, having a temperature at its lower operating end, was circulated through the engine cooling system until the coolant in/coolant out temperatures stabilized and became equal. Then the engine was started and run for several hours at idle speed, maintaining the low coolant outlet temperature. Afterward, the engine block was disassembled and both visual and optical examinations were made of every liner and piston. No sign of scuff was evident according to the opinion of experienced crew members servicing the test stand.

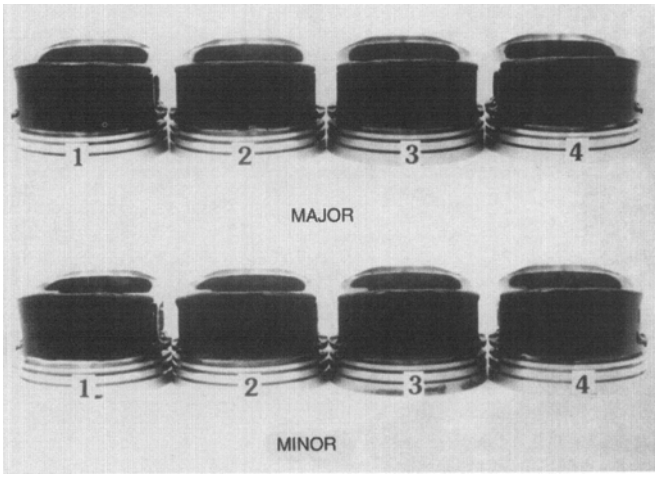

Fig. 27 Photographs of pistons after the cold scuff test

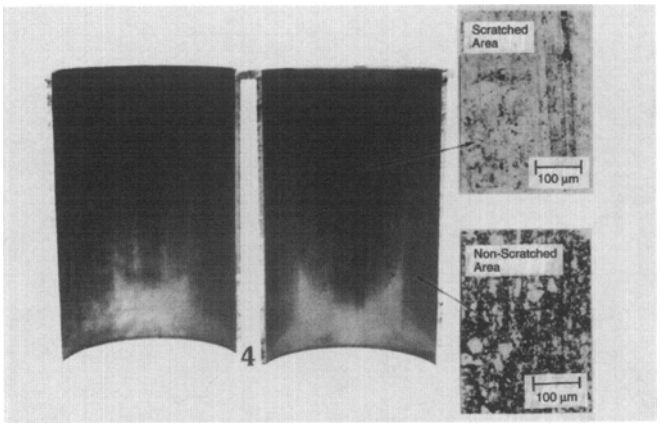

Fig. 28 Optical micrographs of the discolored area on liner #4 after the cold scuff test, showing minor scratching on the liner, possibly due to silicon removal from the etched A390 liner (liner diameter approx. 7.5 cm)

Figure 27 shows the skirt areas of the pistons after the test. The 1.5 μm DLHC applied to the portion of pistons below the ring grove line are evidently intact. Similar examination of the surface condition of the liners indicated areas of discoloration. The cause of that may be scratching or polishing due to some loose particles, possibly silicon grains, released from the etched A390 liner surface during sliding. These loose particles may have become trapped between the liner and the piston skirt, causing scratching on the liner surface. Micrographs in Fig. 28 show the scratched area on liner #4 compared with the non-discolored area. To further investigate the cause of discoloration, SEM micrographs were taken from the discolored zone (Fig. 29a) and compared to the original surface (Fig. 29b). From these micrographs, it is seen that the discolored spots are areas where the silicon grains were either pulled out or polished during sliding. These silicon particles then caused the scratching evident in the photograph. It is also clear that no scuffing occurred. Three-dimensional topography would provide further information as to how much topographical change actually occurred.

Due to the "life expectancy" of a modern combustion engine, which is measured in tens of years or hundreds of thousands of miles, a persistent wear environment in which a piston operates would most likely require DLHCs thicker than that tested in our first dynamometer test. To address this issue, a second dynamometer test was carried out with 5 μm thick DLHC-coated pistons. The adhesion tests with coatings up to 7 μm (see Fig. 14) indicate that sufficient performance should be achieved with relatively thick DLHCs. Nevertheless, the

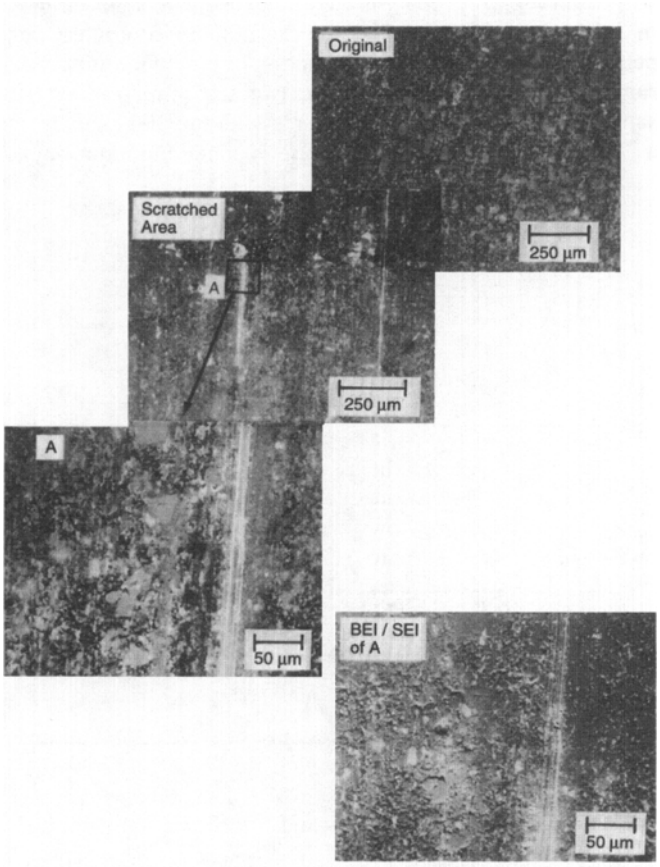

Fig. 29 SEM micrographs detailing the nature of scratching on the liners

layer's overall tribological performance, aside from being dependent on the deposit's adhesion, is also a function of the morphology of the DLHC. Depending on the coating's morphology it may be, for example, more or less abrasive for the mating surface. Microstructural control of the DLHC falls into the still-developing area of manipulation of "primitive growth" structures obtained by altering parameters in a plasma environment, such as chemical composition, target bias, gas density, etc. (see, e.g., Ref 21, 22). Since the control of coating stress (which affects its adhesiveness) and microstructure require manipulation of the same processing parameters, our 5 μm DLHC reported here, despite its high adhesion, differed in its microstructure. Consequently, subsequent dynamometer tests run with 5 μm DLHC-coated pistons indicated the existence of wear beyond what we consider the test passing standard. In addition, some other (than coating) system components were altered, which makes the whole experiment even less conclusive. Beyond any doubt, especially when addressing automotive industry quality standards (and component reliability and reproducibility), the whole processing recipe requires further research that will lead to full control of the coating's stress and morphology so as to meet the requirements of particular commercial applications.

7. Conclusions

Ion bombardment modification of surfaces is an emerging technology which finds application whenever control of surface chemistry, microstructure, and residual stress can affect the service performance of the treated material. This initial study of the potential of surface modification as a means of improving the tribological properties of aluminum automotive components may be summarized in the following:

- Due to continuous wear, even the best-performing submicron surface modification seems to be insufficient for automotive component applications since, specific to this industry, the components are expected to survive over a long time with poorly defined environmental conditions and quite often unreliable maintenance. Potential for submicron surface modifications seems to be limited to applications requiring short-lived, continuous service, and to maintenance-free special applications such as military or aerospace ones where the life of the component is limited and the expected top performance could be a one-time event.
- Because of the shallow penetration depth of the implanted ions, the largest improvements in tribological properties are observed in cases where implantation results in a change of the wear mode. Then, in applications with a well-defined threshold level separating faulty operation from reliable performance, ion implantation may bring about a qualitative change.
- Since deposition of surface coatings by vacuum techniques produces modified layers which are two orders of magnitude thicker than the depth of ion implantation, hybrid processes involving coatings and implantation should be considered instead.
- We have partly verified that such a hybrid approach, involving a diamond-like hydrocarbon coating and ion implantation on aluminum pistons, results in pistons that can pass a preliminary cold scuff test when run in an aluminum block without a cast iron liner. The process appears to be economically scaleable to mass production levels. A subsequent test, however, has shown that process control problems have yet to be worked out, and the process as a whole is far from being ready for commercialization.

Acknowledgments

The authors extend their sincere thanks to Dennis Meyers, Yucong Wang, Robert VanTol, and Chester Rivard for their support in making the engine test possible. Our thanks are also due to Peter Vernia for his contribution in the development of the Cameron-Plint test and to Raymond Lints for his help in doing SEM work. We also would like to acknowledge Richard Waldo for the microprobe analyses and Steve Simko and Maria Militello for AES analyses.

References

1. B. Appleton, B. Sartwell, P. Peercy, and R. Schaffer, *Mater. Sci. Eng.*, Vol 70, 1985, p 23
2. G.S. Was, *Prog. Surf. Sci.*, Vol 32, 1989, p 211
3. J.K. Hirvonen and C.R. Clayton, in *Surface Modification and Alloying by Laser, Ion and Electron Beams*, Plenum Press, 1983, p 323
4. G. Dearnaley, *Nucl. Instr. Meth.*, Vol 182/183, 1981, p 899
5. J.R. Conrad, J.L. Radtke, R.A. Dodd, F.J. Worzala, and N.C. Tran, *J. Appl. Phys.*, Vol 62, 1987, p 4591
6. W.A. Reass, *J. Vac. Sci. Technol. B*, Vol 12 (No. 2), 1994, p 854
7. W.A. Reass, "Optimal Pulse Modulator Design Criteria for Plasma Source Ion Implanters," paper presented at the 9th IEEE International Pulse-Up Power Conference, 21-23 June, 1993, Albuquerque, NM
8. R.R. Speth, G.A. Emmert, and M.J. Goeckner, *Appl. Phys. Lett.*, Vol 65 (No. 18), 1994, p 2272
9. E. Rabinowicz, *Friction and Wear of Materials*, John Wiley and Sons, 1965
10. B. Bhushan and B.K. Gupta, *Handbook of Tribology*, McGraw Hill, 1991
11. C. Subramanian, *Wear*, Vol 151, 1991, p 97
12. S. Ohira, K. Hei, and M. Iwaka, *Nucl. Instr. Meth.*, Vol B32, 1988, p 66
13. T. Kimura, S. Kgaiyma, and S. Yogo, *Thin Solid Films*, Vol 94, 1982, p 191
14. R.E. Clausing, L.L. Horton, J.C. Angus, and P. Koidl, Ed., *Diamond and Diamond-like Films and Coatings*, NATO ASI Series B, Physics, Vol 266, Plenum Press, 1991, p 193
15. J.W. Rabalais and S. Kasi, *Science*, Vol 239, 1988, p 623
16. N. Kichuchi, T. Komatsu, and H. Yoshimura, *Mater. Sci. Eng. A*, Vol 105-106, 1988, p 623
17. R. Wei, P.J. Wilbur, A. Erdemir, and F.M. Kustas, *Surf. Coat. Technol.*, Vol 51, 1992, p 139
18. R. Wei, P.J. Wilbur, M. Liston, and G. Lux, *Wear*, Vol 162-164, 1993, p 558
19. A. Erdemir, M. Switala, R. Rei, and P.J. Wilbur, *Surf. Coat. Technol.*, Vol 50, 1991, p 17
20. G. Malaczynski et al., U.S. Patent 5,458,927, 17 Oct 1995
21. S.M. Rossnagel, J.J. Cuomo, and W.D. Westwood, Ed., *Handbook of Plasma Processing Technology*, Noyes Publications, 1989
22. R.E. Clausing, L.L. Horton, J.C. Angus, and P. Koidl, Ed., *Diamond and Diamond-like Films and Coatings*, NATO ASI Series B, Physics, Vol 266, Plenum Press, 1991